glass capillary tubes was exposed to sunlight for 60 days. After this time the colorless liquid phase turned yellow and a gray residue deposited on the walls. These observations suggest photolytic decomposition. This presents another interesting and useful feature of this compound for the electronics industry as $InNp_2Me$ could be used to deposit a thin indium film directly onto a substrate by a laser-assisted decomposition.

Since $InNp_2Me$ was a volatile liquid that was readily purified by distillation and might possibly be a useful starting material for making semiconductor films, an attempt was made to synthesize $InNpMe_2$ from $InNpCl_2$ and LiMe in a 1:2 mol ratio in Et_2O at −78 °C. After the reaction was complete, removal of the last traces of Et_2O proved difficult. The organoindium product was then partially separated from LiCl by pentane extraction. However, the liquid product so obtained was observed to produce small amounts of solid LiCl upon standing at 25 °C. This observation suggests the presence of $LiInNpMe_2Cl \cdot n Et_2O$. Repeated pentane extractions produced a colorless liquid from which more LiCl formed. Vacuum distillation was then used to separate a volatile organoindium compound from LiCl. However, ^1H NMR spectra demonstrated that the ratio of neopentyl to methyl groups was not one to two as required by the formula $InNpMe_2$. Thus, it was not possible to obtain a pure sample of $InNpMe_2$ by using this preparative procedure. A redistribution/symmetrization reaction as shown by eq 2 apparently occurred during distillation. Thus, it is of

$$2InNpMe_2 \rightarrow InNp_2Me + InMe_3 \quad (2)$$

significance that we were able to distill $InNp_2Me$ and obtain an analytically pure product. Either $InNp_2Me$ does not redistribute/symmetrize or the appropriate experiment that might define the occurrence of a redistribution/symmetrization reaction has not been investigated.

Acknowledgment. This work was supported in part by the Office of Naval Research. The National Science Foundation, Chemical Instrumentation Program, provided funds used to purchase the diffractometer.

Registry No. $InNp_3$, 106136-98-5; InI_3, 13510-35-5; NpMgCl, 13132-23-5; $InNp_2Cl$, 120666-40-2; $InCl_3$, 10025-82-8; $InNpCl_2$, 120666-41-3; $InNp_2Me$, 120666-42-4; $InNpMe_2$, 120666-43-5; $InNp_3 \cdot NMe_3$, 120666-44-6; $InNp_3 \cdot$TMEDA, 120666-45-7; $InNpCl_2 \cdot NMe_3$, 120666-46-8; $InNpCl_2 \cdot$TMEDA, 120666-47-9; $InNp_2Me \cdot$THF, 120666-48-0; $InNp_2Me \cdot NMe_3$, 120666-49-1; $InNp_2Me \cdot$TMEDA, 120666-50-4; $[InNp_2Me]_2 \cdot$TMEDA, 120666-51-5; $(InNp_2Cl)_2$, 120666-52-6.

Supplementary Material Available: Tables of thermal parameters and least-squares planes (3 pages); a listing of observed and calculated structure factor amplitudes (3 pages). Ordering information is given on any current masthead page.

Reactivity of Alkynes toward M–η^2-CS_2 Metal Complexes. 2. A Theoretical Discussion on the Coupling Products Obtainable with Iron Fragments and Their Relative Stability

Jing Li,[1] Roald Hoffmann,*[,1] Carlo Mealli,*[,2] and Jérôme Silvestre[3]

Istituto di Stereochimica ed Energetica dei Composti di Coordinazione, CNR-Via J. Nardi 39, 50132 Florence, Italy, and Department of Chemistry, Cornell University, Ithaca, New York 14853, and Rhône-Poulenc Agrochimie, BP 9163-69263, Lyon Cedex 09, France

Received November 23, 1988

Complexes of the type $(CO)_2(PR_3)_2Fe$–η^2-CS_2, known to yield different coupling products with alkynes, are studied. In particular two products, the metallocycle L_4Fe–C(S)C(R)C(R)S and the 1,3-dithiol-2-ylidene L_4Fe–CSC(R)C(R)S, isomerize easily and, for an appropriate choice of the phosphine ligands, are in equilibrium. Extended Hückel calculations and qualitative MO theory are used to analyze the electronic features of these compounds and their possible interconversion pathways. The study illustrates the major orbital effects and, indirectly, the electrostatic effects that may become selective at a certain point of the reaction.

Introduction

After about 20 years of experimental and theoretical work it is now well established that the reactions of coordinated CO_2 and CS_2 are governed by a complex interplay of factors.[4] One would like to elucidate the subtle correlation existing between charge and orbital control of their reactivity and to learn how geometrical rearrangements govern their reactions. The use of semiempirical methods[5] accounts poorly for the electrostatic effects. On the other hand, the use of more sophisticated methods[6] does not allow the flexibility necessary to test all of the effects over a large range of geometric rearrangements. The nature of the metal fragment, the mode of coordination, and the amount of bending of the triatomic itself determine a plethora of conditions which is difficult to untangle. While it has become clearer that the reactivity of CO_2 is significantly charge-controlled, that of CS_2 is more likely to be monitored by evolution of the frontier MOs. Discussions of various coordination modes of met-

(1) Cornell University.
(2) ISSECC, CNR.
(3) Rhône-Poulenc Agrochimie.
(4) (a) Butler, I. S.; Fenster, A. E. *J. Organomet. Chem.* **1974**, *66*, 161. (b) Baird, M. C.; Hartwell, G., Jr.; Wilkinson, G. *Inorg. Phys. Theor.* **1967**, 2037. (c) Fenster, A. E.; Butler, I. S. *Inorg. Chem.* **1974**, *13*, 915. (d) Le Bozec, H.; Gorgues, A.; Dixneuf, P. H. *J. Am. Chem. Soc.* **1981**, *100*, 2486. (e) Grundy, K. R.; Harris, R. O.; Roper, W. R. *J. Organomet. Chem.* **1975**, *90*, C34. (f) Collins, T. J.; Roper, W. R.; Town, K. G. *J. Organomet. Chem.* **1976**, *121*, C41. (g) Fachinetti, G.; Floriani, C.; Chiesi-Villa, A.; Guastini, C. *J. Chem. Soc., Dalton Trans.* **1979**, 1612. (h) Bianchini, C.; Mealli, C.; Meli, A.; Orlandini, A.; Sacconi, L. *Inorg. Chem.* **1980**, *19*, 2968. (i) Touchard, D.; Le Bozec, H.; Dixneuf, P. H. *J. Organomet. Chem.* **1978**, *156*, C29. (j) Southern, T. G.; Oehmichen, U.; LeMarouille, J. Y.; Le Bozec, H.; Grandjean, D.; Dixneuf, P. H. *Inorg. Chem.* **1980**, *19*, 2976. (k) Herberhold, M.; Süss-Fink, M.; Kreiter, C. G. *Angew. Chem., Int. Ed. Engl.* **1977**, *16*, 193.

(5) Mealli, C.; Hoffmann, R.; Stockis, R. *Inorg. Chem.* **1984**, *23*, 56.
(6) (a) Sakaki, S.; Kitaura, K.; Morokuma, K. *Inorg. Chem.* **1982**, *21*, 760. (b) Sakaki, S.; Dedieu, A. *J. Organomet. Chem.* **1986**, *314*, C63.

0276-7333/89/2308-1921$01.50/0

al–CS_2 complexes can be found in literature,[7,8] the most common being the η^2 form η^2-CS_2.

As a part of a project assessing the bonding capabilities and reactivity of carbon disulfide, we have already presented a study of the coupling of two alkyne molecules on a Rh–η^2-CS_2 system.[9] The subject is far from being exhausted, as other interesting cycloadditions with activated alkynes, which have a sure potentiality in organic syntheses, need to be explored. For example, the cycloaddition may give several different products, such as the heterocyclic five-membered metalla ring complex,[10] **1**, or the metal–dithiocarbene (1,3-dithiol-2-ylidene) complex[11] **2**, or the recently reported alternative five-membered metallacyclic structure **3**.[12]

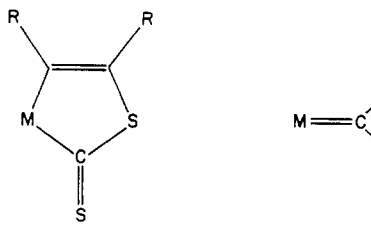

1

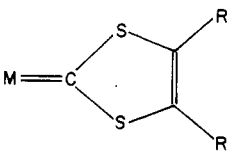

2

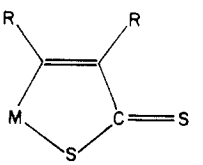

3

Dixneuf et al. have reported the isomerization of **2** to **1** for the $(CO)_2L_2Fe$–η^2-CS_2 complex (L = phosphine).[13] The equilibrium between **1** and **2** is reached when L is chosen to be PMe_2Ph, whereas isomerization from **2** to **1** takes place when L is a more electron-donating ligand, for example, PMe_3. The stable form of **2** exists only with relatively less electron-donating L group, such as $P(OMe)_3$. According to these experimental observations, the hypothesis has been made[7] that the metal–1,3-dithiol-2-ylidene complex **2** and metallacyclic ring **1** are energetically comparable and that the two reactions are in competition.

The purpose of the present study is to explore in some detail the reaction pathways leading to **1** and **2**, and how their interconversion becomes possible. A theoretical analysis of the molybdenum species **3**,[12] which presents some analogies with the iron compounds, will be presented in a subsequent paper as an appendix to the detailed report of its chemistry.[14] All the molecular orbital analysis is performed at the extended Hückel level.[15]

Discussion

M(η^2-CS_2): The Precursor. The general features of the MO's for the L_nM–η^2-CS_2 coordination mode are well-known.[8] These can be constructed by using the familiar fragmentation analysis.[16] In the following discussion we refer to the interaction between orbitals of a typical d^8 L_4M fragment[17] and the CS_2 molecule.[18] The metal fragment here is $(CO)_2(PH_3)_2Fe$, but for simplicity we have used hydride in place of PH_3 ligands.[19]

Only a single symmetry plane (xy) characterizes the molecule. Thus the MO interaction diagram is divided into σ (in-plane) and $\pi_\perp$ subsets, shown in **4** and **5**, respectively.

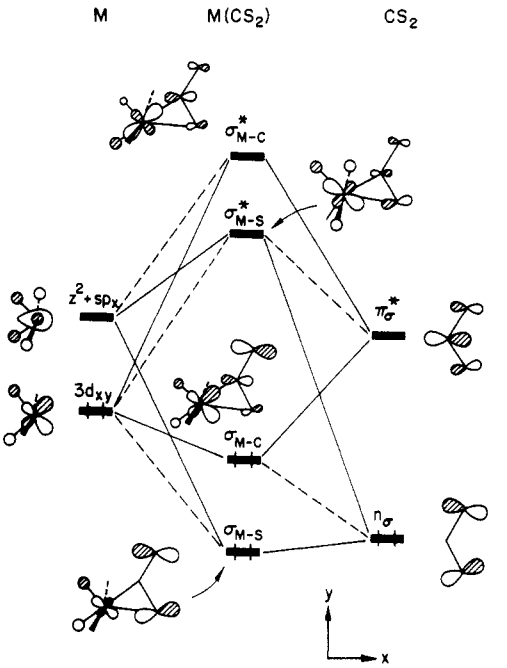

4

In **4**, two important in-plane metal FMOs need to be focused on. The HOMO of the metal fragment **6a** has a major contribution from Fe $3d_{xy}$ and is filled with two electrons for a d^8 L_4M species.

(7) Bianchini, C.; Mealli, C.; Meli, C.; Sabat, M. *Stereochemistry of Organometallic and Inorganic Compounds*; Bernal, I., Ed.; Elsevier: Amdterdam, 1986; Vol. 1, pp 146–254.

(8) (a) Le Bozec, H.; Dixneuf, P. H.; Carty, A. J.; Taylor, N. *J. Inorg. Chem.* **1978**, *17*, 2568. (b) Conway, P.; Grant, S. M.; Maning, A. R. *J. Chem. Soc., Dalton Trans.* **1979**, *1920*. (c) Mealli, C.; Hoffmann, R.; Stockis, A. *Inorg. Chem.* **1984**, *23*, 56. (d) Bianchini, C.; Masi, D.; Mealli, C.; Meli, A. *Ibid.* **1984**, *23*, 2838.

(9) Bianchini, C.; Mealli, C.; Meli, A.; Sabat, M.; Silvestre, J.; Hoffmann, R. *Organometallics* **1986**, *5*, 1733.

(10) (a) Wakatsuki, Y.; Yamazaki, H.; Iwasaki, H. *J. Am. Chem. Soc.* **1973**, *95*, 5781. (b) Le Bozec, H.; Gorgues, A.; Dixneuf, P. H. *Inorg. Chem.* **1981**, *20*, 2486.

(11) (a) Le Marouille, J. Y.; Lelay, C.; Benoit, A.; Grandjean, D.; Touchard, D.; Le Bozec, H.; Dixneuf, P. H. *J. Organomet. Chem.* **1980**, *191*, 133. (b) Schenk, W. A.; Schwietzke, T.; Müller, H. *J. Organomet. Chem.* **1982**, *232*, C41. (c) Reference 5b. (d) Le Bozec, H.; Gorgues, A.; Dixneuf, P. H. *J. Am. Chem. Soc.* **1978**, *100*, 3946. (e) Gorgues, A.; Le-Coq, A. *Tetrahedron Lett.* **1979**, *50*, 4829. (f) Bianchini, C.; Meli, A. *J. Chem. Soc., Chem. Commun.* **1983**, 1309. (g) Bianchini, C.; Meli, A.; Scapacci, G. *Organometallics* **1985**, *4*, 264. (h) Frazier, C. C.; Magnussen, N. D.; Osuji, L. N.; Parker, K. O. *Organometallics* **1982**, *1*, 903.

(12) Conan, F.; Guerchais, J. E.; Mercier, R.; Sala-Pala, J.; Toupet, L. *J. Chem. Soc., Chem. Commun.* **1988**, 345.

(13) (a) Reference 9b. (b) Le Bozec, H.; Gorgues, A.; Dixneuf, P. H. *J. Chem. Soc., Chem. Commun.* **1978**, 573.

(14) Conan, F.; Sala-Pala, J.; Guerchais, J. E.; Mercier, R.; Toupet, L.; Li, J.; Hoffmann, R.; Mealli, C. *Organometallics*, following paper in this issue.

(15) (a) Hoffmann, R.; Lipscomb, W. N. *J. Chem. Phys.* **1962**, *36*, 2179, 3489. **1962**, *37*, 2878. (b) Hoffmann, R. *Ibid.* **1963**, *39*, 1397.

(16) (a) Hoffmann, R.; Swenson, J. R.; Wan, C.-C. *J. Am. Chem. Soc.* **1973**, *95*, 7644. (b) Fujimoto, H.; Hoffmann, R. *J. Phys. Chem.* **1974**, *78*, 1167.

(17) Albright, T. A.; Burdett, J. K.; Whangbo, M.-H. *Orbital Interactions in Chemistry*; Wiley: New York, 1985, pp 394–401.

(18) Gimarc, B. M. *Molecular Structure and Bonding*; Academic Press: New York, 1979.

(19) The interatomic distances between Fe and C and between Fe and endocyclic S are taken to be 2.0 and 2.36 Å respectively, comparing to those found in $(CO)_2(PMe_3)(PPh_3)$Fe–η^2-CS_2, 1.98 and 2.33 Å, respectively.[4a] For the two C–S bonds, an average value of 1.65 Å is used. Other geometrical parameters used in the computations are summarized in the Appendix.

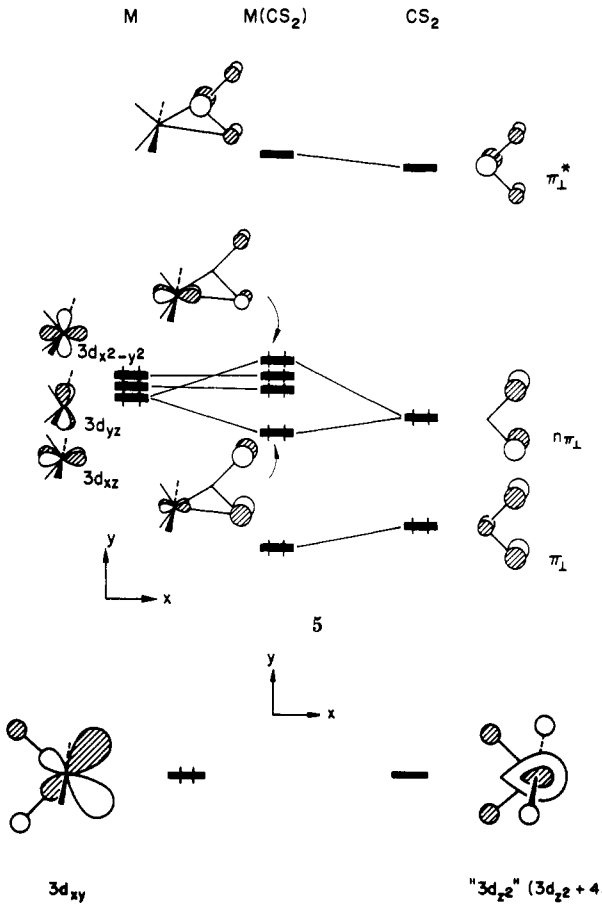

This orbital is suitable for donation of electrons to the high-lying CS_2 orbital, π_σ*, **7a**, which is greatly concentrated on the carbon atom, for electronegativity reasons. The back-donation from the metal results in a strong σ-type Fe–C bond during the rehybridization process. An overlap population of 0.35 is computed between the two interacting orbitals. Notice that the description of the Fe–C bond as due to metal π-back-donation implies that no metal oxidation occurs in M-η^2-CS_2 coordination. The forward donation to the metal fragment comes mainly from n_σ, **7b**. This CS_2 orbital is completely localized on the two

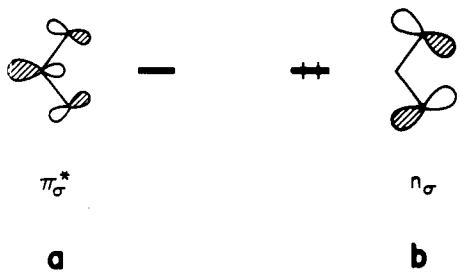

sulfur atoms. It overlaps with the empty metal z^2, **6b**, to form a Fe–S bond. Upon interaction, the z^2 orbital loses its original character (both in σ_{M-C} and σ_{M-C}* levels). A real mixing of $3d_{z^2}$ and the 4s and $4p_x$ hybrid of iron takes place in these orbitals.

The often invoked analogy to the Dewar–Chatt–Duncanson description of metal–olefin bonding[20] is here an

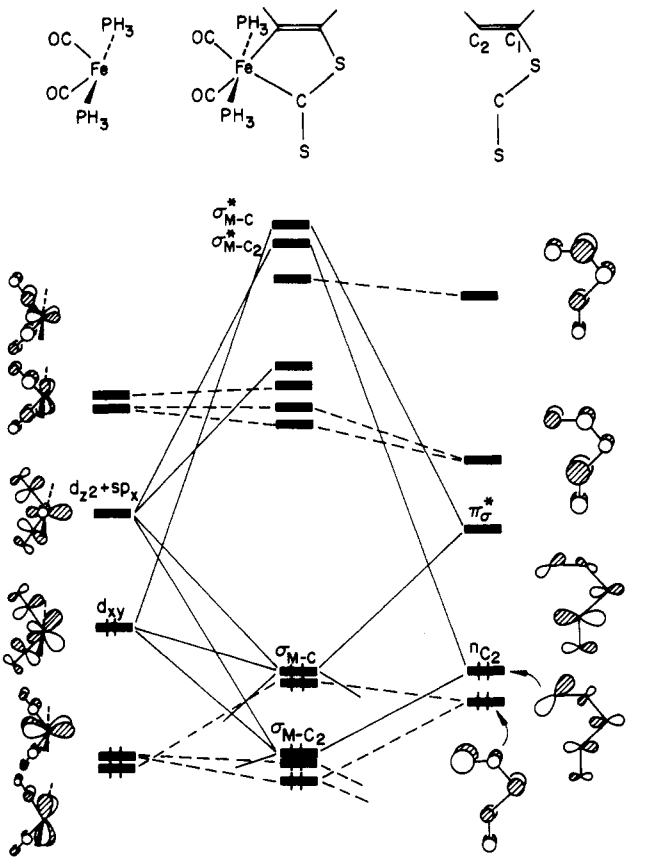

Figure 1. Schematic interaction diagram for the formation of the five-membered metallacycle **1**. The d^8 ML_4 fragment orbitals are shown at left and those of the $(CS_2)(C_2R_2)$ at right.

oversimplification, though, a useful one. Lack of symmetry forces mixing between σ and π components. The HOMO, labeled σ_{M-C} in **4**, is distributed over three centers; its composition of 42% of Fe $3d_{xy}$, 40% of π_σ*, and about 10% of n_σ from CS_2 results in a large lobe on the exocyclic sulfur atom. A redistribution of electron density must accompany the large MO delocalization. Electrons, donated from metal to carbon, become extensively localized on the exocyclic sulfur atom (S_{exo}). This is computationally verified, with a calculated net gain of 0.3 electron by the latter atom. The accumulation of the electron density on S_{exo} makes this atom a site of electrophilic attack. When a easily polarizable alkyne reacts with the so formed metal-η^2-CS_2 complex, it is very likely that the alkyne directs a positively charged end to S_{exo}. Notice that this way of envisaging reactivity, most typical for ionic VB structures, is here based on MO and perturbation theory arguments.

Interactions of $\pi_\perp$-type, sketched in **5**, are much weaker. The low-lying orbitals, $n_{\pi_\perp}$ from CS_2 and $3d_{xz}$ from metal, give rise to a two-orbital/four-electron interaction pattern. The result is a slight destabilization. The empty $\pi_\perp$* on CS_2 does not find an appropriate partner to interact with and stays almost unaffected. It remains a potential center of electrophilicity. The suggestion is that the four $\pi_\perp$ electrons of CS_2 remain equally distributed over the two C–S linkages. This may not be entirely true as the $\pi_\perp$ cloud is affected by the unequal distribution of changes created by the σ electron density distribution. Experimentally, the exo C–S bond is found to be shorter than the endo one, whereas there is no trace of this in the calculated C–S overlap populations, which are practically equal. If the four $\pi_\perp$ electrons are ideally subdivided in a lone pair and in a double bond, the former is expected to localize opposite to the sulfur atom containing the σ lone

(20) (a) Chatt, J.; Duncanson, L. A. *J. Chem. Soc.* **1953**, 2939. (b) Dewar, M. J. S. *Bull. Soc. Chim. Fr.* **1951**, *18*, C79.

pair. More double-bond character is attributed to the exocyclic C=S linkage. Pictorially, structure **8a** is assigned a larger weight than **8b**.

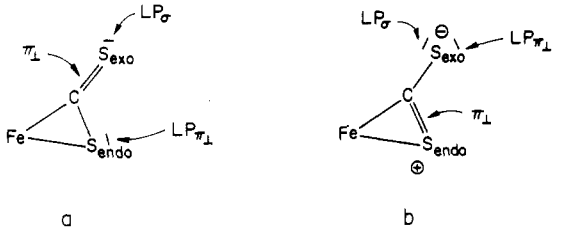

8

Formation of the Metallacycle 1. As mentioned early, reaction of an activated alkyne with $(CO)_2L_2Fe$–η^2-CS_2 gives two products, the metalla ring complex **1** or the metal–dithiocarbene complex **2**, depending on the choice of the L group.[13] The two processes, labeled A and B, respectively, are schematized in **9**. In the present section we will focus on the formation of the metalla ring structure, i.e. process A, and leave the discussions of process B for the next section.

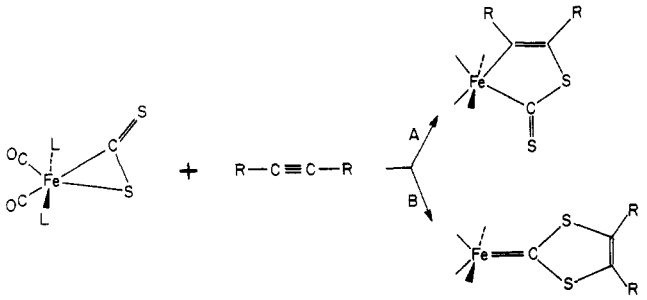

9

A simplified interaction diagram for the formation of the five-membered metallacycle **1** is shown in Figure 1. One of the carbon atoms from the alkyne, C_2, forms a bond with the metal, and the other, C_1, is bonded to exocyclic sulfur. The d^8 L_4Fe fragment orbitals are shown on the left and those of $CS_2C_2H_2$ grouping at right.

Since we are dealing with a low-symmetry system, great mixing among the orbitals under consideration is expected. But the main feature is clear: there are four important fragment orbitals, the two familiar metal d^8 L_4M frontier orbitals d_{xy} and $(d_{z^2} + sp_x)$ at the left and the π_σ* and n_{C_2} at the right in the figure. Notice that π_σ* has still much of the character of the π_σ* level of the bent CS_2 and is concentrated on CS_2 carbon atom (see **4**), while n_{C_2} is nonbonding and mostly on C_2. Given the relative energies of the four interacting orbitals, the σ_{M-C_2} bond originates from the two electrons donated from n_{C_2} into the empty $d_{z^2} + sp_x$ metal hybrid. By contrast, the σ_{M-C} bond can still be regarded as a sort of back-donation from d_{xy} to π_σ* (d_{xy} is lower than π_σ*). Again, the $\pi_\perp$-type interactions do not contribute significantly to bonding and are not further discussed. The overlap populations calculated for the σ_{M-C} and σ_{M-C_2} are 0.284 and 0.233, respectively, and can be compared with the 0.35 value found in the Fe–η^2-CS_2 precursor.

We have described the bonding in metallacycle **1** in its ground-state geometry. Obviously, there are many possible routes to the final structure, three of which are sketched in **10**. It is reasonable to assume that all approaches are likely to be confined within the *xy* symmetry plane.[21] In

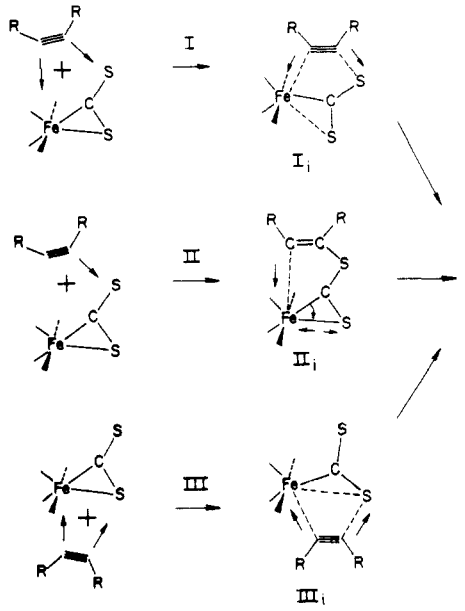

10

route I the two carbons of the acetylene are brought toward Fe and S_{exo} atoms at the same "rate". In route II, C_1 approaches to the uncoordinated S at a faster "pace" to form an intermediate of some sort, II_i. Along route III, C_1 approaches to S_{endo}, which is much less negatively charged than S_{exo}. Therefore, an electrophilic attack should be difficult at this site.

The computed high energy of the transition state for this route III suggests that such a pathway is unfavorable toward the cycloaddition. Although energetically comparable, route II seems more realistic than I due to the strong nucleophilicity of the exocyclic sulfur atom. We have found that when an activated (nonlinear) alkyne is brought close to the two sulfur, as shown in **11**, the S_1–C_1 bond is formed much faster than the S_2–C_2 bond. This is not surprising, since it is the electrophilic attack that actually occurs at the early stage of the process.

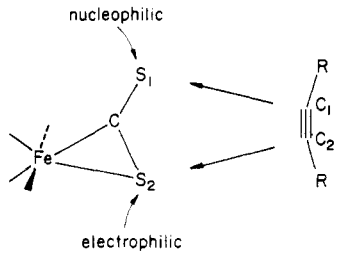

11

The route we then follow is II, drawn in **10**. First, C_1 of an acetylene derivative is brought in toward S_1 of Fe–η^2-CS_2 to form a C–S bond. This causes some electron transfer to the second acetylene atom, C_2, favoring the formation of a lone pair on it. This is the analogue of n_{C_2} in Figure 1. Hence C_2 steps in. The formation of the Fe–C_2 bond and the breaking of the Fe–S bond are carried out simultaneously.

To simplify the problem of disentangling the corresponding Walsh diagram of Figure 2, we discard the orbitals which are antisymmetric with respect to the mirror plane ($\pi_\perp$). The starting point, at the left side, is II_i, and the final product is the metallacycle **1**. The solid lines are the actual connections between the starting and the ending orbitals, and dashed lines represent the intended correlations. Let us take a close look at the two σ orbitals at the left side. These are a lone pair on C_2 (LP_{C_2}) and a Fe–C

(21) We have compared the situation in which C_2R_2 approaches $FeCS_2$ complex in the *xy* plane to that where it approaches sideways from above; the result clearly shows that the coplanar approach is energetically favored.

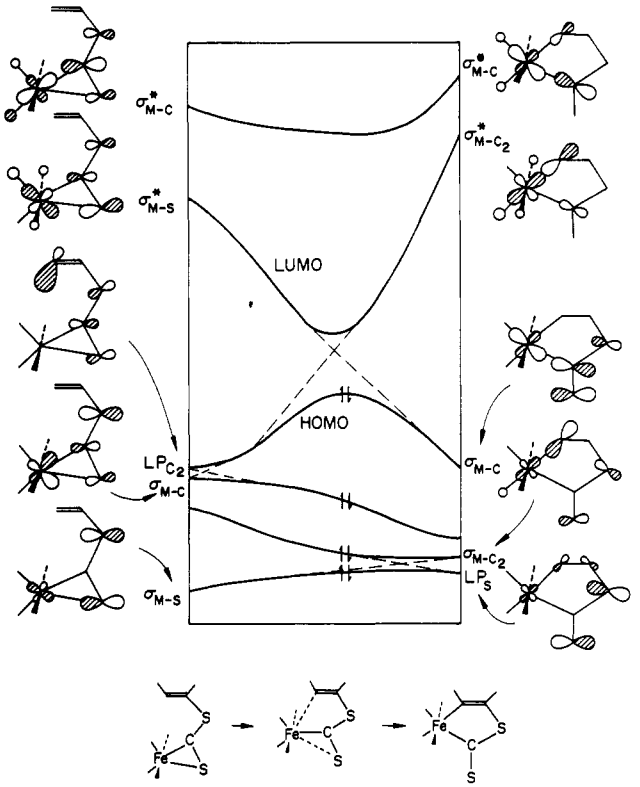

Figure 2. Walsh diagram correlating II_i and the metallacycle 1. The corresponding orbitals are sketched in the figure. The avoided crossings are represented by dotted lines. The geometrical variables associated with the process are listed in the Appendix.

σ bond (σ_{M-C}). In the early stages of the reaction, C_2 is far away from the metal and there is very little interaction between the two atoms. Therefore, LP_{C_2} intends to stay unchanged. However, the σ_{M-C} level rises up rapidly, due to the loss of overlap between Fe and C. An avoided crossing takes place with the two levels repelling each other while mixing their character. Then, at the midpoint of the reaction pathway, a HOMO–LUMO avoided crossing occurs. This corresponds to the conversion of CS_2 to a η^1-coordination mode. As shown in **12**, the LUMO becomes

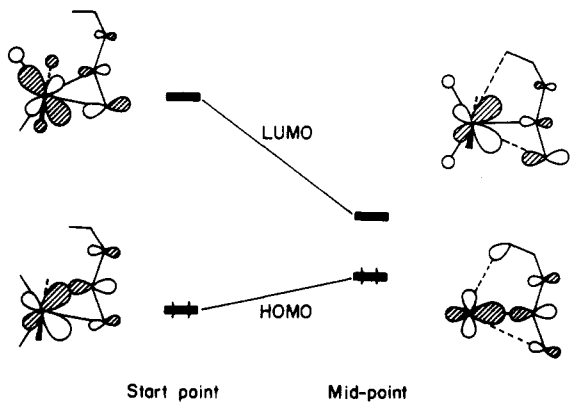

12

much concentrated on Fe $3d_{xy}$ (d_π) and the HOMO is very similar to the Fe–C σ-bonding orbital in metal–carbene complexes.[22] In the present case, however, the instability of the midpoint geometry is clear. It is best regarded as a transition state rather than an intermediate. In fact the d_π orbital, which should provide a stabilizing back-donation, is empty.

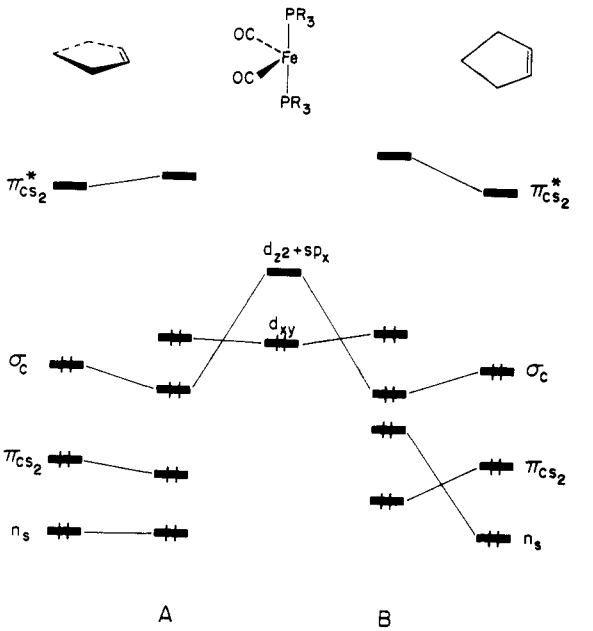

Figure 3. Correlation diagram showing the orbitals and the relative shifts for the two configurations **13a**(**A**) and **13b**(**B**).

Moreover the HOMO–LUMO gap is too small. Implicitly the divergence between HOMO and LUMO levels on both the left and the right side of the Walsh diagram can be regarded as a way of overcoming a second-order Jahn–Teller instability of the system in the η^1-coordination geometry.[23] For $(CO)_2(PH_3)_2Fe$-η^2-CS_2 + C_2H_2 we compute a 0.97 eV barrier for the process. The product ring structure is stabilized by 1.0 eV with respect to II_i.

Formation of the Metal–1,3-Dithiol-2-ylidene Complex. The electronic nature of metal-η^1-1,3 dithiol-2-ylidene models has been discussed elsewhere.[9] In looking for the stable conformers there are two choices, **13a** (equatorial, in-plane) or **13b** (upright).

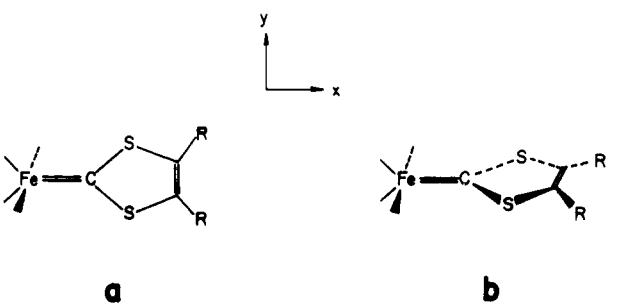

13

At first glance one might think that **13b** is more favorable, since with this geometrical arrangement one could utilize the Fe $3d_{xy}$ to overlap with π_{CS_2}*, whereas an interaction of this kind is not possible in the equatorial geometry **13a**. It turns out, however, that **13a** is much more stable than **13b**, giving an energy difference of more than 3 eV. Why is this so? An explanation may be found in Figure 3. The left side of figure shows how **13a** is formed.

A strong bonding interaction between metal (z^2 + sp_x) (empty) and the σ_C orbital from the CS_2–C_2H_2 ring (filled) produces a Fe–C σ bond. An overlap population of 0.4 is obtained. In **13a** the metal $3d_{xy}$ and π_{CS_2}* are orthogonal and there is essentially no π-type stabilization from the

(22) Hofmann, P. *Transition Metal Carbenes*; Verlag Chemie; Weinheim, 1983; pp 113–180.

(23) Jahn, H. A.; Teller, E. *Proc. R. Soc. London, Ser. A* 1937, *A161*, 220.

two fragments. In this respect configuration **13b** might be expected to ensure the right interaction between the latter two FMOs. This is not so because of the large energy gap and also because the expected $3d_{xy}-\pi_{CS_2}^*$ bonding is compensated by a two-orbital/four-electron destabilizing interaction of $3d_{xy}$ and π_{CS_2}. Moreover, the close contact between sulfur and phosphorus atoms causes a strong repulsion, **14**, which is reflected in the Figure 3 by a large increase in energy of n_S, the sulfur lone-pair orbital.

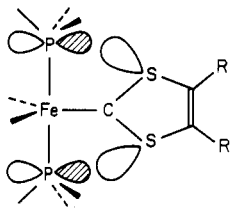

14

Bending back the phosphorus atom can diminish such repulsion (see **15**). At the same time one of the lower metal orbitals, $3d_{xz}$, will be greatly destabilized because of the built-in of the antibonding character between this orbital and the phosphorus lone pair.

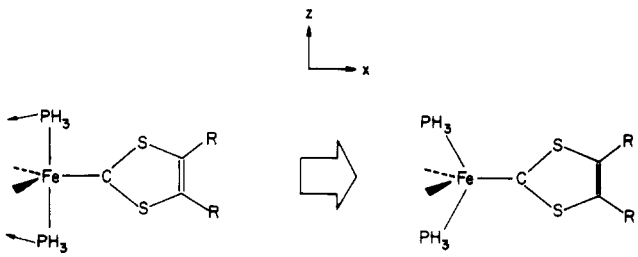

15

This is drawn in **16**. As a result, the metal fragment itself is to a great extent destabilized and so is the whole molecule. In any event, the computed rotational barrier for this carbene complex appears surprisingly high and other geometrical rearrangements may occur. For example a Berry pseudorotation process can go through a more favorable tbp structure with the carbene ligand in the axial position, but no computation has been performed.

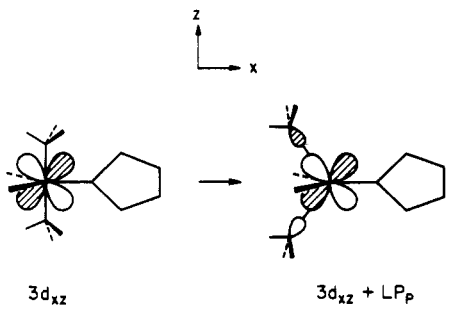

16

Noticeably, in the structure of the Fe–carbene–$HgCl_2$ adduct, $HgCl_2$–$Fe(CO)_2(PMe_2Ph)_2(CS_2)(C_2R_2)$[24] (**17**), the

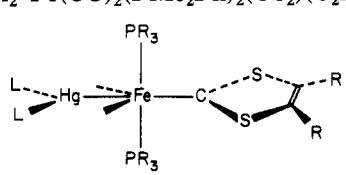

17

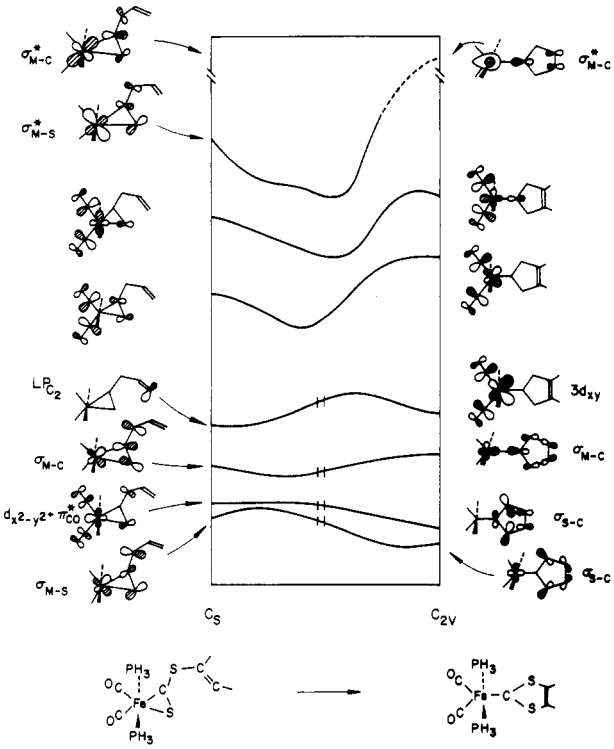

Figure 4. Walsh diagram for the process illustrated in **18**. The orbitals of the starting geometry are drawn on the left side of the figure and those of the final product, on the right side. The geometrical variables associated with the process are listed in the Appendix.

1,3-dithiol-2-ylidene ring lies in the same plane as the CO ligands, thus confirming that a structure of type **13a** is favored. Due to the lack of suitable $\pi_\perp$ back-donation in the L_4M–carbenoid complex, a filled metal d_{xy} orbital (HOMO) and an empty CS_2 π^* are forced to coexist in a dipole of some sort. Further reactivity of this species is then expected. It could be exhibited toward a dipolarophile (a second alkyne molecule) or an acidic metal center ($HgCl_2$).

Pathways leading to the 1,3-dithiol-2-ylidene ring have been previously outlined.[9] An important one is the 1,3-dipolar cycloaddition.[25-28] On the basis of argument made early, we consider the mechanism where the addition and cyclization are constrained to the symmetry plane. The possibility of a suprafacial addition is not excluded[6] but will not be discussed here. Figure 4 is a Walsh diagram for the process pictured in **18**.

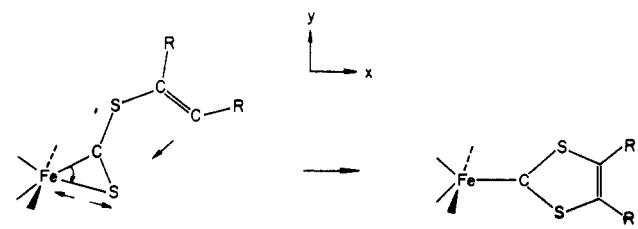

18

A few points concerning the initial and final structures need to be illustrated. Only those orbitals symmetric with

(24) Le Bozec, H.; Dixneuf, P. H.; Adams, R. D. *Organometallics* **1984**, *3*, 1919.

(25) Houk, K. N.; Sims, J.; Duke, R. E.; Strozier, R. W.; George, J. K. *J. Am. Chem. Soc.* **1973**, *95*, 7287.
(26) Huisgen, R. *Angew. Chem., Int. Ed. Engl.* **1963**, *2*, 633.
(27) Fleming, I. *Frontier Orbitals and Organic Chemical Reactions*; Wiley: New York, 1976; pp 148–161.
(28) Pearson, R. G. *Symmetry Rules for Chemical Reactions*; Wiley: New York, 1976; p 364.

respect to the *xy* plane are shown.

Similar to the formation of metallacycle 1, electrophilic attack at the exocyclic sulfur is likely to be the first step of the reaction. If so, the *dangling* alkyne of the fragment Fe-η^2-$(CS_2)(C_2H_2)$ (**19a**) must have the opportunity to rotate freely from one to the other side of the exocyclic C–S bond. A negligible energy barrier is expected for the interconversion **19a** → **19b**.

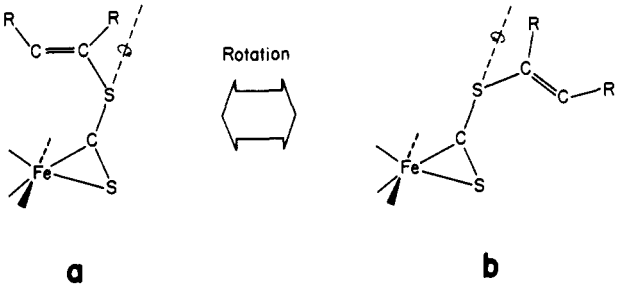

19

As shown in **20**, the only MO that contributes to create a barrier is largely metal d_{xz} centered, with a small contribution from a π orbital of the $(CS_2)(C_2H_2)$ grouping. As the alkyne group is rotated out of *xy* plane (along the $C–S_{exo}$ axis) the π-bonding overlap between C_1 and S_{exo} becomes partially antibonding, causing a small rise in energy until it reaches the halfway point of the reaction. The HOMO of the complex, also shown in **20**, is unaffected, as it is the lone-pair orbital localized on C_2.

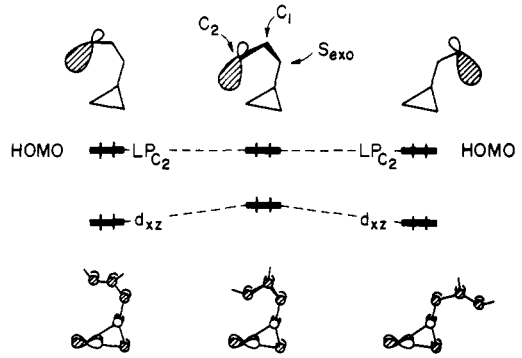

20

On the right side of Figure 4, the SCS angle in the final η^1-ring structure has been optimized. The best value is achieved for angles between 100 and 115°. Combining the experimental data of 108.7° for $Cp(CO)(P(OMe)_3)Mn–[CS_2C_2(CO_2Me)_2]$[11a] and of 112.5° for $Cl_2Hg–(CO)_2(PMe_2Ph)_2Fe–[CS_2C_2(CO_2Me)_2]$,[23] with the consideration of avoiding too short S–S contact, we choose an angle of 115° for the final geometry. We can then proceed to draw the actual connections between orbitals at the starting and ending point in Figure 4. The intended correlations are summarized in **21**. As expected, there are many avoided crossings and great orbital intermixing. σ_{M-C} intends to go up at the start of the reaction due to the immediate weakening of the overlap between metal *xy* and CS_2 π_σ* orbitals. The lone pair on C_2 intends to stay put in energy, thus an avoided crossing occurs between the two and the slopes of the two curves are reversed.

Midway in the reaction, a new orbital, originally metal $d_{x^2-y^2} + \pi_{CO}$* in character, mixes with the descending level. Eventually, the metal–sulfur bonding orbital σ_{M-S} and the LP_{C_2} become the two carbon–sulfur σ-bonding orbitals, and σ_{M-C} correlates to metal $3d_{xy}$, a filled but nonbonding orbital at the final geometry. The barrier for the process is calculated to be 0.90 eV, and a stabilization of 0.65 eV is gained going from left to the right.

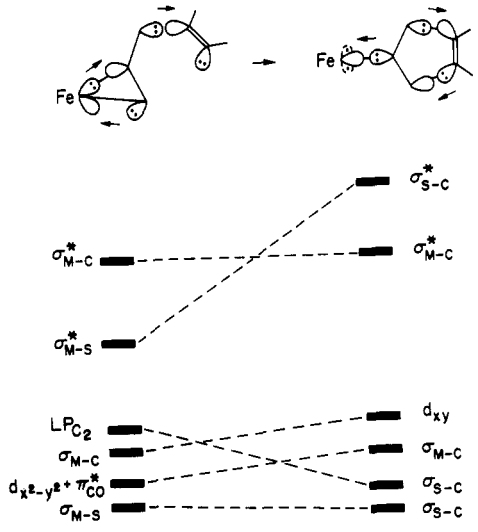

21

As illustrated at the top in **21**, we can follow the fate of the electrons along the reaction. Ultimately, of the three original C–C bonding pairs of the alkyne, one (the π in-plane one) is transferred as a lone pair to the CS_2 carbon atom which becomes a strong σ donor. The metal does not change oxidation state but, much less involved in back-donation, is now richer with electrons.

Metallacycle versus Metal–Carbene Complex. The two processes for the formation of the metallacycle 1 and metal–carbene complex **2** from the η^2-CS_2 precursor are energetically comparable, giving a modest barrier of 0.97 and 0.90 eV, respectively. Both structures are stabilized with respect to their starting point, i.e. the specimen where a dangling alkyne is attached to the S_{exo} atom. An energy difference of 0.3 eV is calculated for the two species. Thus, the barrier for the interconversion of the two structures is similar in both cases, and this accounts for the reported equilibrium. At this point we wonder what is the effect of different phosphine ligands, in shifting the equilibrium toward one form or the other. We have performed calculations with different L groups in $(CO)_2L_2Fe(CS_2)(C_2H_2)$ adducts, e.g. L = PH_3 or PF_3. The quantitative results for the two processes do not show any significant change either in the barrier or in the pattern of MO evolution. In other words, different choices of the PR_3 groups do not seem to introduce any sensible orbital control of the reaction. Our feeling is that the differences in reactivity are imposed by a charge effect that can be traced indirectly by using qualitative arguments.

The EHMO method calculates a net metal charge of –0.6 electron in the compound **1** but a much more negative value (–1.1) in 1,3-dithiol-2-ylidene derivative. As mentioned, the large difference is mainly due to the absence of back-donation in the latter. Thus, in metal-carbene the iron atom is willing to accept ligands that are more electron-withdrawing species. Or to put it in another way, the dithiocarbene structure is stabilized by electron-withdrawing coligands. Another piece of evidence for the basicity of the metal in complex **2** is the ability to form donor–acceptor adducts of type **17** with a Lewis acid such as $HgCl_2$.[24] Why can the compound $Cl_2Hg–(CO)_2(PMe_2Ph)_2Fe–[CS_2C_2(COOMe)_2]$ be isolated easily and studied by single-crystal X-ray diffraction, while its precursor is not? We have already illustrated the reasons why configuration **13a** is more stable than **13b**, in spite of the potential π-back-donation attainable in the latter. In the absence of such an interaction, the HOMO in **13a** has the character of a largely based d_{xy} orbital significantly de-

Table I. Atomic Parameters Used in the Calculations

atom	orbital	H_{ii}, eV	ζ_1	ζ_2	C_1[a]	C_2[a]
Fe	4s	-9.17	1.90			
	4p	-5.37	1.90			
	3d	-12.7	5.35	1.80	0.5366	0.6678
Hg	6s	-13.68	2.65			
	6p	-8.47	2.63			
	5d	-17.50	6.44	3.03	0.6438	0.5215
P	3s	-18.6	1.60			
	3p	-14.0	1.60			
S	3s	-20.0	1.82			
	3p	-13.3	1.82			
O	2s	-32.3	2.28			
	2p	-14.8	2.28			
C	2s	-21.4	1.62			
	2p	-11.4	1.62			
Cl	3s	-26.3	2.18			
	3p	-14.2	1.73			
H	1s	-13.6	1.30			

[a] Coefficients used in double-ζ expansion for d orbitals.

stabilized by the σ antibonding with the in-plane ligands (see right side of Figure 4). The Lewis acid $HgCl_2$ does not attack directly such a d_π lone pair, but upon geometrical rearrangement of the L_4Fe–dithiocarbenoid complex to a L_5M type of fragment, the latter orbital is greatly depressed. This is a consequence of an improved interaction with π_{CO}* as shown in **22**. At the same time a filled metal σ-nonbonding level, **23** (a member of the 2e set in trigonal-bipyramidal structures) becomes available for interaction with the empty σ orbital of $HgCl_2$. The net energy gain for the system is calculated as large as 3.2 eV.

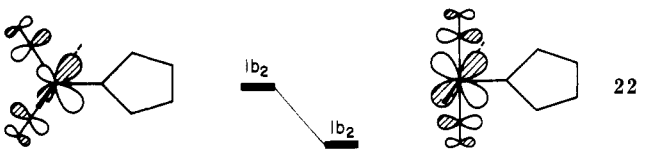

22

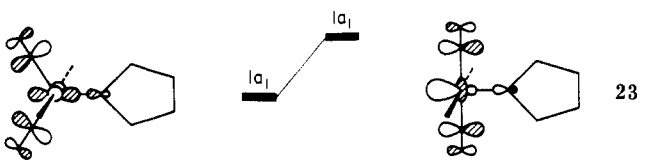

23

Conclusions

In this paper we have tackled the problem of the reactivity of L_4Fe–η^2-CS_2 complexes with activated alkynes. At the end of this report we would like to outline some relevant points which are supported by our MO analysis. The inert CS_2 molecule, often used as a solvent in several inorganic reactions, becomes a powerful nucleophile if properly activated by a metal upon coordination. The charge distribution is consistent with a rehybridization of the frontier molecular orbitals of CS_2. Hence coordinated CS_2 can react with weak Lewis acids such as activated alkynes. The study has suggested that the alkyne is first polarized in presence of the exocyclic sulfur atom (the arguments are based on the increased C–S overlap population) and that a lone pair localizes on the second carbon atom of the alkyne. The lone pair allows electrophilic attack either on the S_{endo} atom (while the M–S bond is cleaved) or on the metal itself to close a metallacycle. The semiempirical method used is not sufficiently reliable to monitor the electronegativity effects of the substituents on the ligands, so as to predict which isomer is favored in which case. However the Mulliken analysis of charge distribution is consistent with the experimental trends reported.

As a final remark, we have no evidence that the formal oxidation state of the metal changes as it does in typical oxidative addition or reductive elimination reactions. In fact, by examining the relative energies of the levels, no electrons originally assigned to the atom of one fragment seem to have transferred to the second fragment. Only some minor electron density shifts are observed. The argument is consistent with a charge-controlled reactivity pattern which is in any case closely related to the orbital rehybridization pattern.

Acknowledgment. We are grateful to NATO for its generous support through Grant No. 200.81 which made this collaboration possible. J.L. would like to express her thanks to the members of ISSECC for their hospitality during her stay in Florence.

Appendix

The extended Hückel approach is employed for the study.[15] The atomic parameters for Fe, Hg, P, S, O, C, and H atoms are tabulated in Table I. Some important geometrical data used in the calculations are listed below.

$(CO)_2(PH_3)_2Fe$–η^2-CS_2 and H_4Fe–η^2-$CS_2)^{4-}$: d(Fe–C(O)) = 1.80 Å, d(Fe–P) = 2.26 Å, d(Fe–C(S)) = 2.0 Å, d(C–S_{exo}) = 1.65 Å, d(C–S_{endo}) = 1.65 Å, d(Fe–H) = 1.70 Å, S_{exo}–C–Fe = 140°, S_{exo}–C–S_{endo} = 140°, Fe–S_{exo}–C = 56.5°, C(O)–Fe–C(O) = 110°, H_{eq}–Fe–H_{eq} = 100°.

$(CO)_2(PH_3)_2Fe(CS_2C_2H_2)$, metallacycle I: d(Fe–C_2) = 2.0 Å, d(S_1–C_1) = 1.65 Å, C_2–C(S)–S_2 = 120°, S_1–C_1–C_2 = 120°.

$(CO)_2(PH_3)_2Fe(CS_2C_2H_2)$, metal–carbene: S_1–C–S_2 = 115°, C–S_1–C_1 = 96.57°.

$HgCl_2$–$(CO)_2(PMe_2Ph)_2Fe$–$[CS_2C_2(COOMe)_2]$: d(Hg–Cl) = 2.5 Å, d(Hg–Fe) = 2.55 Å, Cl–Hg–Cl = 103°.

The following geometrical variables were simultaneously varied at each reaction step to correlate structure II_i and **1** through the Walsh diagram of Figure 2: α, the angle between the horizontal line and the Fe–C bond in II_i; β, the Fe–C–S_2 angle; γ, the C_1–S_1–C angle; and δ, the Fe–C–S_1 angle. The following were simultaneously varied to correlate the two structures reported in **18** and to construct the Walsh diagram of Figure 4: α, the Fe–C–S_1 angle; β, the Fe–C–S_2 angle; γ, the C–S_1–C_1 angle; and δ, the C–Fe–S_2 angle. All bond distances were kept unchanged during both processes.

Registry No. $(CO)_2H_2Fe$-η^2-CS_2, 120966-69-0; $(CO)_2(PH_3)_2Fe$-η^2-CS_2, 110174-32-8; HC≡CH, 74-86-2; $(CO)_2H_2Fe$(C(H)=CHSC(=S)), 120966-70-3; $(CO_2)(PH_3)_2Fe$(CH=CHSC=S), 120966-72-5; $(CO_2)(PF_3)_2Fe$(CH=CHSC=S), 120966-74-7; dicarbonyldihydro(1,3-dithiol-2-ylidene)iron(IV), 120966-71-4; dicarbonyl(1,3-dithiol-2-ylidene)bis(phosphino)iron(II), 120966-73-6; dicarbonyl(1,3-dithiol-2-ylidene)bis(trifluorophosphino)iron(II), 120966-75-8.